Available on CMS information server

CMS NOTE 1998/064

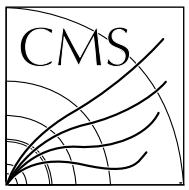

The Compact Muon Solenoid Experiment

CMS Note

Mailing address: CMS CERN, CH-1211 GENEVA 23, Switzerland

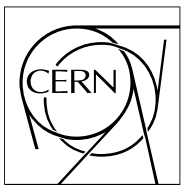

15 October 1998

Performance and mechanical tolerances achieved with a full size prototype of a CMS Barrel Muon Drift Tubes Chamber

S. Bethke, H. Reithler, H. Schwarthoff, V. Sondermann, V. Tano, H. Teykal, J. Tutas, J. Vandenhirtz, H. Wagner, M. Wegner

AACHEN-3A, RWTH, III. Physik. Inst. , Aachen, Germany

A. Benvenuti, G.M. Dallavalle, V.Giordano, C. Grandi, M. Guerzoni, S. Marcellini, A. Montanari, C. Montanari, F.L. Navarria, F. Odorici, A. Rossi, T. Rovelli

Univ. di Bologna e Sez. dell' INFN, Bologna, Italy

M. Aguilar-Benitez, J. Berdugo, M. Cerrada, N. Colino, M. Daniel, M.C. Fouz, P. Ladron De Guevara, J. Mocholi, L. Romero, C. Willmott

CIEMAT, Centro de Investigaciones Energeticas Medioambientales y Tecnologicas, Madrid, Spain

M. Benettoni, E. Conti, M. De Giorgi, A. De Min, U. Dosselli, C. Fanin, F. Gasparini, U. Gasparini, R. Giantin, P. Guaita, I. Lippi, R. Martinelli, A.T. Meneguzzo, M. Pegoraro, A. Sancho Daponte, P. Sartori, E. Torassa, S. Ventura, P. Zotto, G. Zumerle

Univ. di Padova e Sez. dell' INFN, Padova, Italy

M. Arneodo, R. Cirio, F. Daudo, S. Maselli, C. Peroni, A. Staiano

Univ. di Torino e Sez. dell' INFN, Torino, Italy

Abstract

The barrel muon chambers of the CMS experiment are made assembling 3 independent modules (SuperLayers) which together measure the impact point and the angles θ and ϕ. Each SuperLayer consists of four layers of rectangular Drift Tubes. MB96 is a full size prototype of the smallest CMS Barrel Muon Chamber (MB1) built in early 1997 at the Legnaro INFN laboratory and tested in summer 1997 at the CERN CMS test beam facility. The performance of the prototype and the mechanical tolerances achieved in the construction are presented.

1 Introduction

Several barrel muon chamber prototypes of increasing size and number of layers were built in the last three years. Two of them were four-layer systems, $100 \times 64\ cm^2$ and $250 \times 64\ cm^2$ in size. One consisted of 16 layers $50 \times 50\ cm^2$ in area. Two large chambers with twelve layers were also built, one was $1 \times 3\ m^2$, and the second, named MB96, was $2 \times 2.5\ m^2$ like a real MB1 chamber. The prototypes were used to study their performance but also to develop and improve the tools used for the chamber production. Performance and mechanical tolerances achieved with MB96 will be described in the following.

2 The MB96 chamber

The chamber is made of three SuperLayers (SLs) each consisting of four layers of rectangular drift cells staggered by half a cell. The wires in the two outer quadruplets (SL1,SL3) are parallel to the beam line in the CMS reference. In the inner quadruplet (SL2), the wires are orthogonal to the beam line. The chamber is assembled by gluing SL3 with SL2 while SL2 and SL1 are glued to an aluminium honeycomb plate to ensure the required stiffness and increase the lever arm between SL1 and SL3. Fig. 1 shows a corner of MB96, where one sees the 3 SLs, the gas distribution system, the high voltage connectors and the corner blocks carring the reference marks for the position measurements.

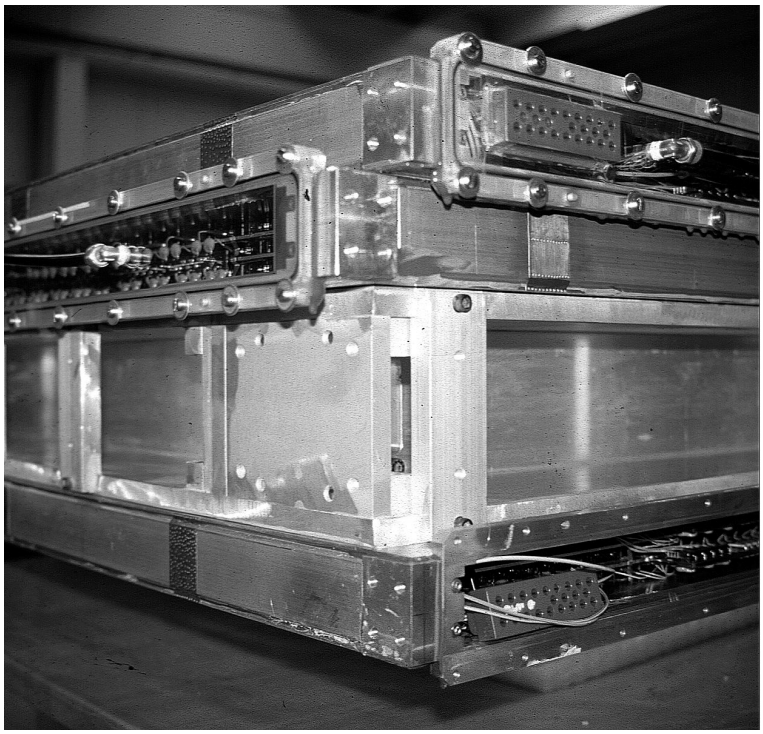

Figure 1: The corner view of the MB96 chamber.

The cell, shown in Fig. 2, has a pitch of $40.0\ mm$ by $13\ mm$. At the center is the anode wire, made out of a $50\ mm$ diameter stainless steel type 304L wire. The cathodes defining the cell width are aluminium I-beams $1.2\ mm$ thick and $9.6\ mm$ high. A plastic profile, made of $0.5\ mm$ thick extruded polycarbonate plastic (Lexan), is glued to the upper and lower parts of the I-beams in order to electrically insulate the cathodes from the aluminium plates (kept at ground potential). A pair of positively-biased strips is placed at the center of the cell above and below the wire. These field shaping electrodes improve the linearity of the space-time relationship. All the prototypes built so far have cells with these dimensions. Fig. 3 shows the exploded view of the end part of few cells: the end-plugs used to position the wires and the contacts used to connect to the HV strips and I-beams.

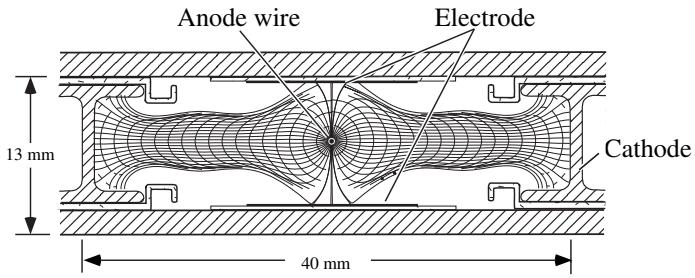

Figure 2: Transverse view of a cell.

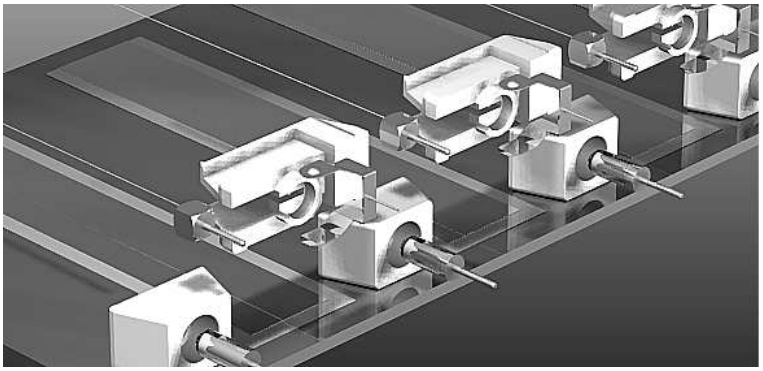

Figure 3: Exploded view of the end part of few cells: the larger plastic end-plugs contain the wire and the strip contacts, the smaller plastic end-plugs are glued to the Al-plane and they define the wire positions.

3 The mechanical precision measurements

The mechanical precision of a chamber is dictated by the aim to achieve the global resolution in (R, Φ), the view measured by SL1 and SL3, of $100\ \mu m$. This figure makes the MB1 chamber precision comparable to the multiple scattering contribution up to $p_t = 200\ GeV$. The $100\ \mu m$ target chamber resolution may be achieved by the 8 track points measured in the two (R, Φ) Super Layers, if the single wire resolution is better than 250 μm. In order to have the global chamber resolution affected mainly by the single wire resolution, the wire pitch tolerance inside one layer and the misalignment between layers in the same superlayers have to be measured with a precision better than $100\ \mu m$ or to be lower than $100\ \mu m$ to avoid the need for a wire position database. Misalignment between Super Layers of the same chamber should be less than $500\ \mu m$ to have signals in the time window of the trigger. It should be measured, during assembly, with at least $100\ \mu m$ resolution. The wire positioning was measured with an optical bar holding a CCD camera (Fig. 4) having $10\ \mu m$ resolution.

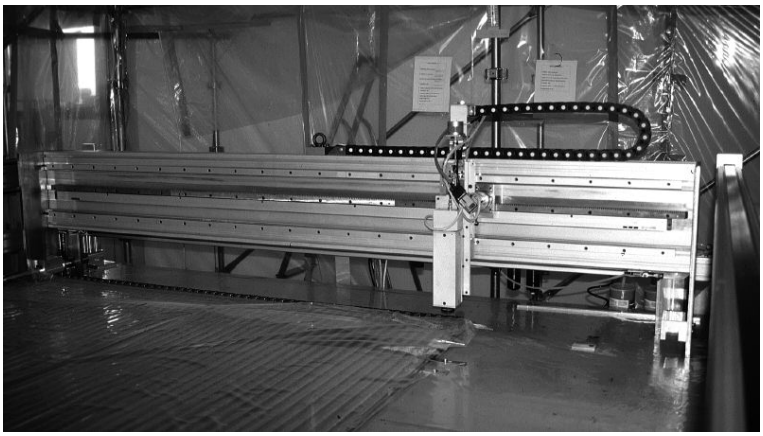

Figure 4: Wire-measuring tool.

The distribution of the wire position w.r.t. the nominal position, measured for each layer at both ends of the wire, for all the cells of the MB96 chamber is shown in Fig. 5. Corrections for temperature difference between measurements and for the shift between layers was applied. The shift between two layers was found to be between 0 and 200 μm depending to the position along the wire and to the layers considered. This systematic error can be reduced with some modification in the tools used for the end plugs and I-beams gluing.

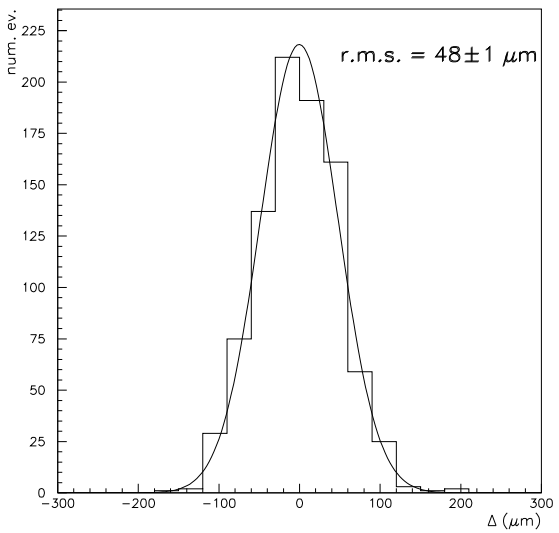

Figure 5: Distribution of the wire distance from the nominal position.

To test uniformity between cells the distribution of the I-beam height including Lexan (Fig. 6) and the distribution of the strip distance from the nominal position (Fig. 7) were measured. The thickness of each superlayer was measured by means of comparators and found to be within $\pm 0.2\ mm$. The global chamber thickness (after 50 superimposed glue joints) was measured to be within $\pm 0.45\ mm$. Some other general checks was done: the wire tension measurement (Fig. 8), the strip contact by measuring the strip capacitance and the gas tightness by measuring the O_2 contamination (30 ppm with the 3 SLs serially connected and a gas flux of 0.2 l/min).

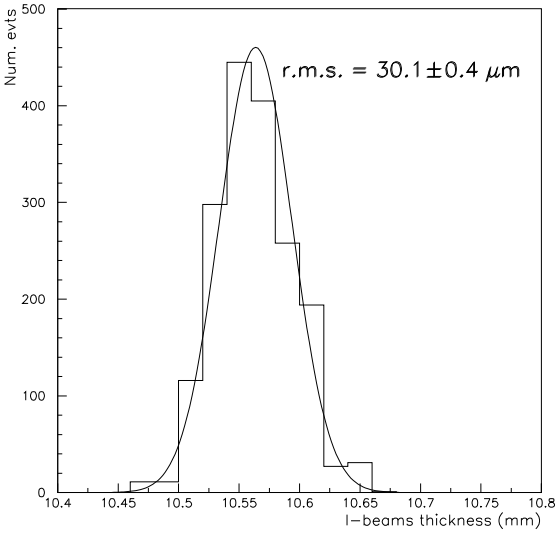

Figure 6: Distribution of the height of the MB96 I-beams made of Aluminium and Lexan.

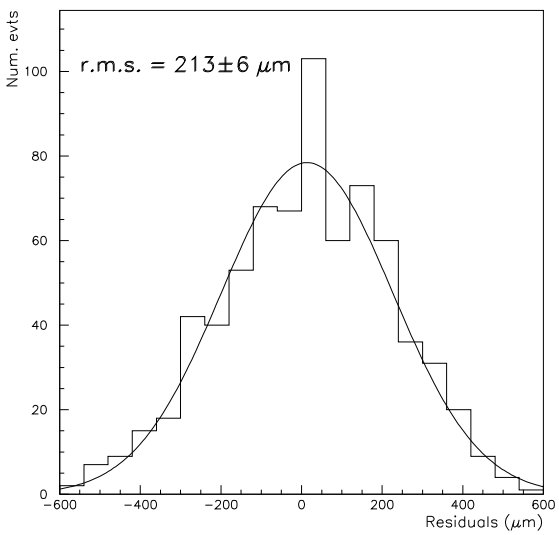

Figure 7: Distribution of the strip distance from the nominal position.

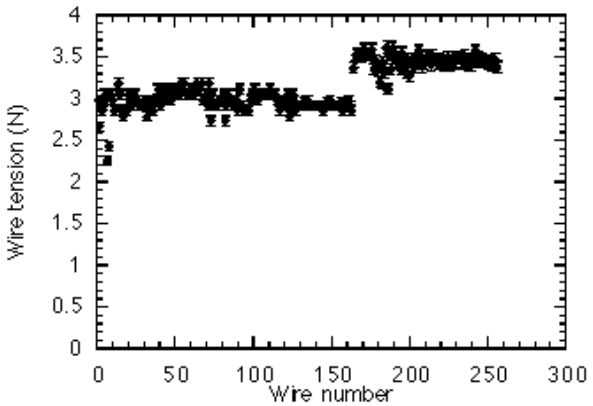

Figure 8: Measured wire tension for some of the wires. The nominal value is 3N. The jump in wire tension coincides with a small change in the mechanics of the crimping machine.

4 Experimental setup

The MB96 chamber was exposed to muon beams with $200 - 300\ GeV$ energy in the H2 test beam area (Fig. 9) at the CERN-SpS during August and September 1997. The chamber was mounted on a support allowing rotations and translations. It was equipped with the ASD-8 amplifier-shaper-discriminator chip [1] and operated with an $Ar(85\%)\ CO_2(15\%)$ gas mixture at different voltages. The gas flux was $0.2\ l/min$ corresponding to 1.5 total volume change per day. An additional H.V. scan was performed with an $Ar(82\%)\ CO_2(18\%)$ gas mixture. The reference H.V. setting (i.e. for the position scan) was:

$$V_{wire} = 3500\,V \qquad V_{strip} = 1700\,V \qquad V_{cathode} = -1700\,V$$

The discriminating threshold was set to $5.5\ fC$. The output signal was then stretched to a width of about $350\ ns$ and buffered at ECL levels. The drift times were digitised with $1\ ns$ resolution by the 32-channel, multi-hit TDC-KLOE VME boards [2], using the common stop mode. The time between the trigger and the common stop was $1\ \mu s$ and the TDC range was $4\ \mu s$. The data used in the analysis described in the next paragraphs were taken with the wires in all SLs orthogonal to the beam line.

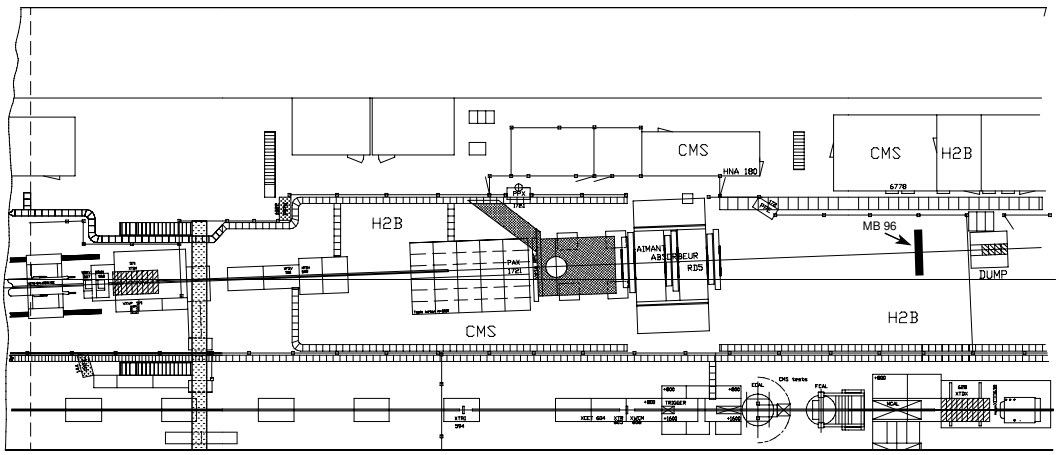

Figure 9: The CMS-H2 area at CERN.

5 Noise

The noise can be random or correlated to the event. Hits generated after a physical hit on a cell are ascribed to correlated noise. These signals can be generated by an electron cluster produced in the cell (i.e. feedback electrons extracted from the cathode by a photon produced during the multiplication process), or by the electronic processing of the physical signals. The first source of correlated noise was eliminated from our measurements by stretching the pulses to $350\ ns$, wich corresponds to the maximum drift time. With our read-out setup the number of double hits was about $2\ \%$ at the reference H.V. setting.

The random noise rate was calculated taking some runs with a random trigger and $32\ \mu s$ of window time. The cosmic rays contribuiton has been removed. The distribution for the SL3 cells is shown in Fig. 10. A similar distribution was found in the Q1 prototype data [3] with the same electronics but stretching the pulses to $80\ ns$.

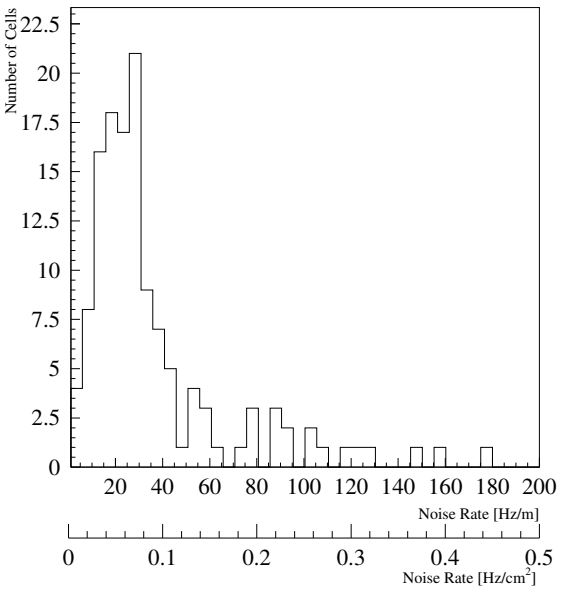

Figure 10: The noise rate distribution for the SL3 cells.

6 Efficiency

The efficiency was measured with a sample of SL3 cells using data taken with the beam orthogonally incident. The sample of events was selected by requiring three or four hits in the SuperLayer under study. A weak cut was applied to the straight line fit (angle less than 30 degree and χ^2 less than 25). The position of the track inside the half-cell was computed in 1 mm bins by interpolation or extrapolation of the fitted trajectory. The efficiency was calculated with the ratio (num. 4 hits)/(num. 4 hits + num. 3 hits). The cell inefficiency as a function of the track crossing position is described in Fig. 11 and Fig. 12. A small efficiency drop occurs in correspondence of the edges of the Lexan strips which isolate the I-beams from the Al planes (Fig. 2). A Similar inefficiency distribution was found in the Q1 prototype data [3] with the peak shifted of about $1.5\ mm$ respect to the distribution for MB96. This shift follows from the smaller width of the MB96 I-beams ($7.2\ mm$) respect to the Q1 I-beams ($9.0\ mm$). The half-cell efficiency was obtained averaging over all bins except the last one. This procedure allows to evaluate the intrinsic cell efficiency inside the geometrical acceptance, and to avoid systematic effects due to non-uniformities inside the cell. The cell efficiency obtained at different voltage settings is given in Fig. 13 as a function of the effective voltage V_{eff}, wich is a quantity proportional to the electric field on the wire surface. V_{eff} is related to the gas amplification M by the relation:

$$M = Ae^{BV_{eff}} \tag{1}$$

and can be parametrised as a function of the voltage settings (in Volts):

$$V_{eff} = (V_w - V_s) + \alpha V_s - \beta V_c \tag{2}$$

$$\alpha = 0.126 \pm 0.002 \qquad \beta = 0.0184 \pm 0.0004 \tag{3}$$

The parameters where determined experimentally through an extensive study of the gas amplification with a radioactive source [5]. The multiplication factor was measured to be about $0.9\ 10^5$ [4]. The dependence of M from V_s (V_c) was obtained with V_c (V_s) and $V_w - V_s$ fixed at $-1950\ V$ and $1800\ V$.

The inefficiency is about 0.12 % in the "plateau" region (above $V_{eff} = 1950$ for $Ar(85\%)\ CO_2(15\%)$ and above $V_{eff} = 2050$ for $Ar(82\%)\ CO_2(18\%)$). The definition of the drift and amplification voltages are the following: $V_{ampl} = V_w - V_s$, $V_{drift} = V_s - V_c$. All the data was taken in the following condition: $V_s = -V_c$

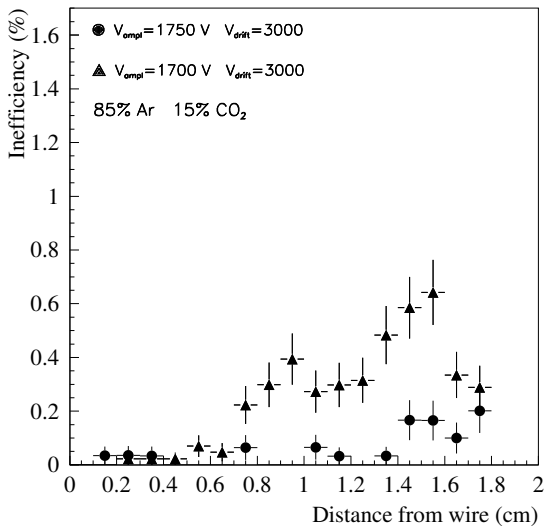

Figure 11: Cell inefficiency as a function of the track crossing position for $Ar(85\%)$ $CO_2(15\%)$ gas mixture and two voltage settings.

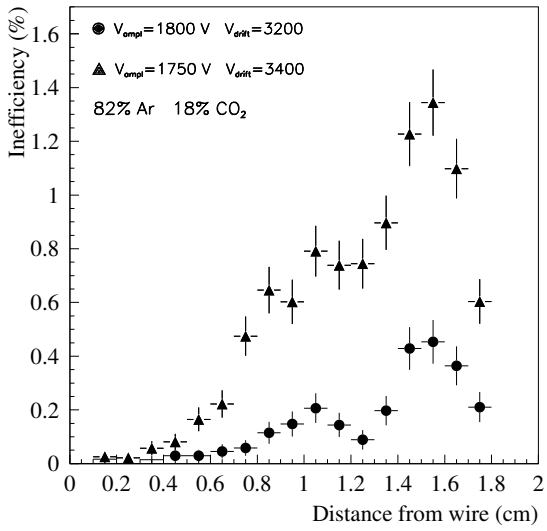

Figure 12: Cell inefficiency as a function of the track crossing position for $Ar(82\%)$ $CO_2(18\%)$ gas mixture and two voltage settings. Note that the voltages used are lower than the reference ones to magnify the inefficiency peak.

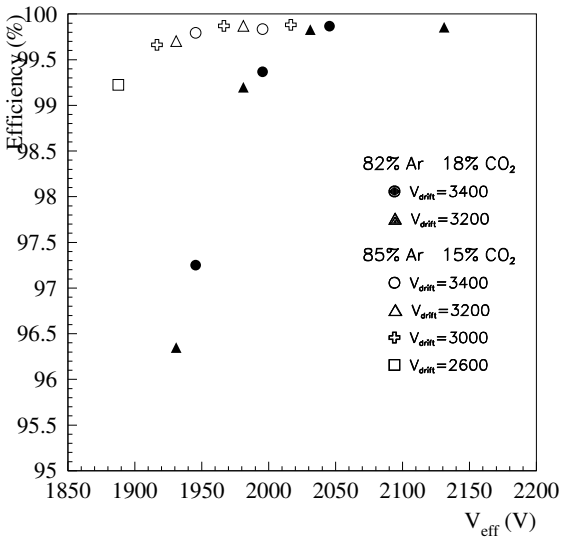

Figure 13: Intrinsic cell efficiency as a function of the effective voltage V_{eff}. The "plateau" regions are shifted of about $80\ V$.

7 Resolution

The mean time variables $MT_j = (t_{j-1} + t_{j+1})/2 + t_j$ where t_j is the drift time measured in layer j, are used to compute the intrinsic cell resolution as $\sqrt{(2/3)} \times R.M.S.(MT_j)$. These variables do not depend on track position and angle if the track crosses a "column" and if the space-time relationship is linear. The result is described in Fig. 14 for some half cells (columns) of the SL3 chamber.

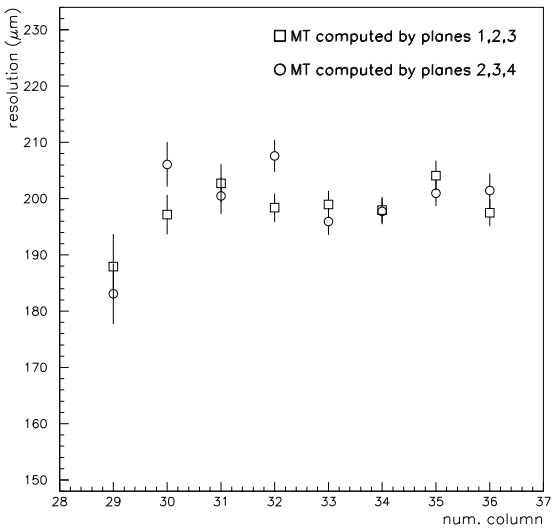

Figure 14: The cell resolution evaluated for some half cells in SL3. The H.V. setting is the reference one.

The resolution can also be evaluated with the residuals from a linear fit in a single SL. The resolution as a function of the beam position is uniform as described for all three SLs in Fig. 15, 16, and 17. The cell resolution in layer j with every points used in the fit is:

$$res._j = \frac{R.M.S.(residuals)_j}{\sqrt{(N-1/N) - (X_j^2 / \sum_{i=1}^{N}(X_i^2))}} \tag{4}$$

where N is the number of points and X_j is the vertical wire position in layer j. The zero reference is the center of the SL. In our case (N=4) the cell resolution is $\sqrt{(10/3)} \times R.M.S.(residuals)$ for the two external layers and $\sqrt{(10/7)} \times R.M.S.(residuals)$ for the internal ones.

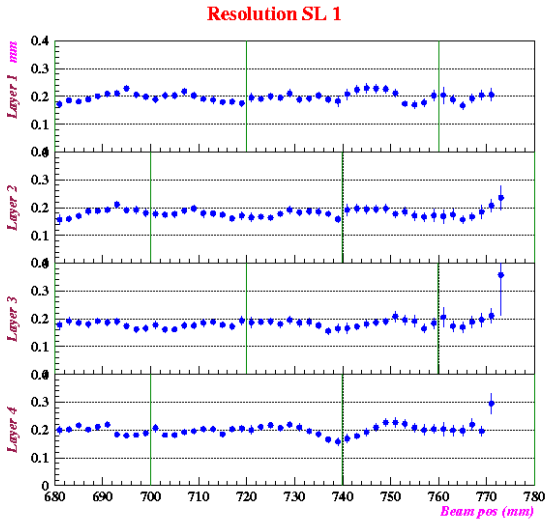

Figure 15: The cell resolution as a function of the beam position in SL1 .

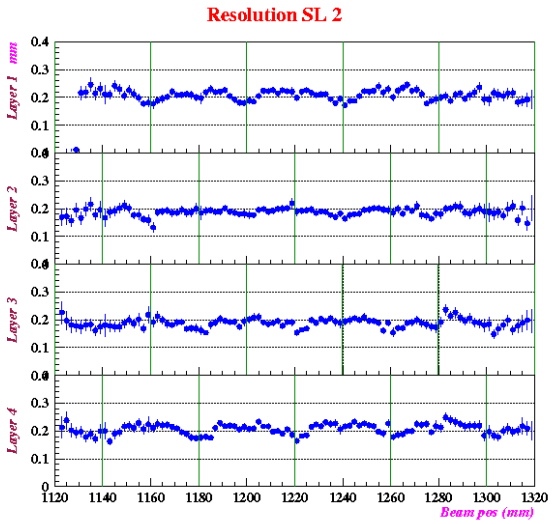

Figure 16: The cell resolution as a function of the beam position in SL2.

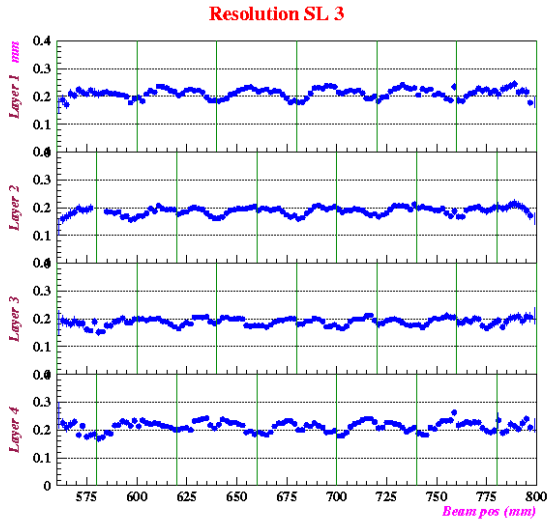

Figure 17: The cell resolution as a function of the beam position in SL3.

8 Efficiency at the end of the wire

To test the efficiency in proximity of the plastic end-plugs a fine scan in the last 30 mm close to the end of the wire was performed. A scintillator hodoscope 0.8 mm large allowed to reach a resolution of $\pm 0.5 mm$. The position $x = -5$ mm is the beginning of the wire, $x = 0$ mm correspond to the wire emerging from the plastic end-plug (beginning of the strip). The I-beam cathodes start at $x = 5$ mm. Fig. 18 shows that the cell already reaches full efficiency at $x \simeq 8$ mm. In the full efficiency region there's no distortion in the drift time (Fig. 19).

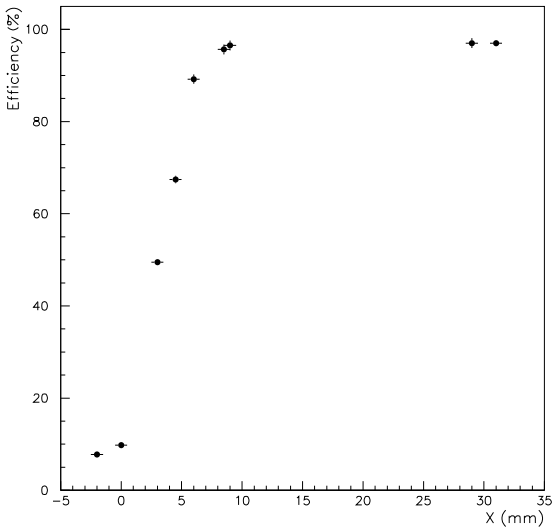

Figure 18: Efficiency as a function of the coordinate along the wire.

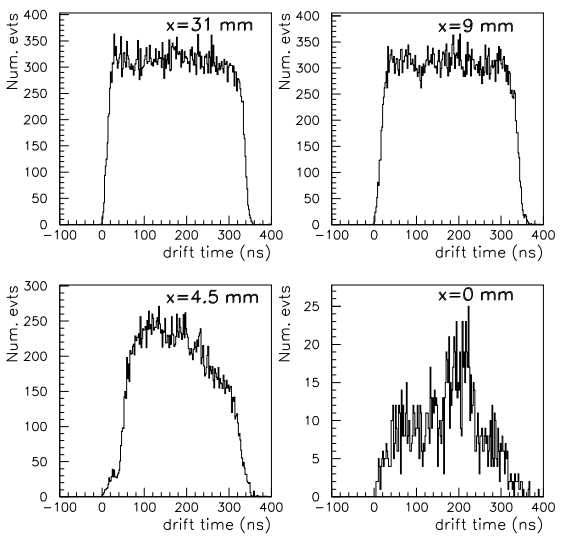

Figure 19: Drift time boxes for different positions along the wire.

9 Conclusions

The prototype chamber MB96 fulfils the mechanical tolerance requirements. Only the shift between two layers in the wire positioning has to be fixed. The chamber tightness is good: the O_2 contamination during the testbeam was about 30-50 ppm with 1.5 volume change per day. The inefficiency is very low, 0.12%, when the chamber is operated at the reference voltage. The cell resolution is about $200\ \mu m$ and is uniform over the chamber. The cell already reaches full efficiency at about $8\ mm$ from the point where the wire emerges from the plastic end-plug.

References

[1] F.M. Newcomer et al., IEEE Trans. Nucl. Sci., 40(1993) 630.

[2] M. Passaseo, E. Petrolo, S. Veneziano, *A TDC integrated circuit for drift chamber readout.* Nucl. Instr. Meth. A 367 (1995) 418-421.

[3] S. Bethke et al., *Performance of the Drift Tubes for the Barrel Muon Chambers of the CMS Detector at LHC.* Nucl. Instr. Meth. A. 410 (1998) 133-147.

[4] E. Conti, R. Giantin, F. Gonella, M. Pegoraro, E. Torassa, *Experimental tests of the Q2 Drift Tubes prototype chamber for the CMS Muon Barrel.* CMS NOTE 1997/019

[5] E. Conti, private communication.